

Structure of Flux Lines in Three-Dimensional Layered Type-II Superconductor: Numerical Experiments

Masahiko Machida* and Hideo Kaburaki

Computing and Information Systems Center, Japan Atomic Energy Research Institute,
Tokai-mura, Ibaraki, 319-11, Japan

(Received 4 March 1994)

We clarified the vortex structure of modeled 3D type-II layered superconductors by solving directly the time dependent Ginzburg-Landau equation coupled with the Maxwell equation. We found, in both modeled type-A ($d \approx \xi_c$) and type-B ($d \gg \xi_c$) systems, where d and ξ_c are a layer periodicity and a coherence length in the c axis, respectively, stable entangled vortex structures near the sample edge by the external field inclined with respect to the c axis. By increasing the temperature in the modeled type-B system, we also found a change from straight to staircase vortices consisting of segments parallel and perpendicular to layers.

PACS numbers: 74.60.Ec

High temperature superconductors have layered structures consisting of superconducting two-dimensional CuO_2 planes and other planes which are not directly related to superconductivity. These intrinsic multilayered structures have a great influence on vortex structures [1,2]. Among high- T_c materials, due to the differences of a coupling between CuO_2 planes, the anisotropy is small in $\text{YBa}_2\text{Cu}_3\text{O}_7$ (YBCO), while it is very large in $\text{Bi}_2\text{Sr}_2\text{CaCu}_2\text{O}_x$ (BSCCO). It has been shown experimentally that these characteristics give rise to differences in vortex structures [3,4].

In this Letter, a direct numerical simulation [5,6] of the coupled system of the time-dependent Ginzburg-Landau (TDGL) equation [7] and the Maxwell equation has been made on the two types of three-dimensional layered superconductors to study the effect of layered structures on vortex structures. No numerical studies have been reported so far on three-dimensional vortex states using a complete set of the TDGL equation and the Maxwell equation except for simplified models derived from the GL theory. We report the numerical results of anomalous vortex solutions of the above equations under the presence of layered structures.

Two characteristic parameters should be considered in modeling multilayered superconductors [8]. One is the coherence length ξ_c for the c axis and the other is the length of the unit cell of the crystalline lattice d in the c axis in which strong and weak superconducting layers are stacked. These parameters ξ_c and d characterize the spatial variation of the order parameter and the periodicity of the layered structure, respectively. In general, when $\xi_c \approx d$, the effect of superconducting coherence prevails over the layer periodicity effect. On the other hand, when $\xi_c \ll d$, the layered structure becomes a very important factor. In this Letter, the model is referred to type-A when $\xi_c \approx d$, and type-B when $\xi_c \ll d$. Here, $\xi_c(0)$ denotes the coherence length at zero temperature and d corresponds to the periodicity of the variation T_c as shown

schematically in Fig. 1. Therefore in the type-A model, since the strong superconducting layers are considered to be highly coupled, the layered structure has little effect on three-dimensional vortex structures. On the other hand, in the type-B model, due to weak coupling between strong superconducting layers, the vortex structures tend to be easily modified.

The model equations which are employed for direct numerical simulation are as follows:

$$D^{-1} \left(\frac{\partial}{\partial t} + i \frac{2e\varphi}{\hbar} \right) \Delta + \xi^{-2} (|\Delta|^2 - 1) \Delta + \left(\frac{\nabla}{i} - \frac{2e}{\hbar c} \mathbf{A} \right)^2 \Delta = 0,$$

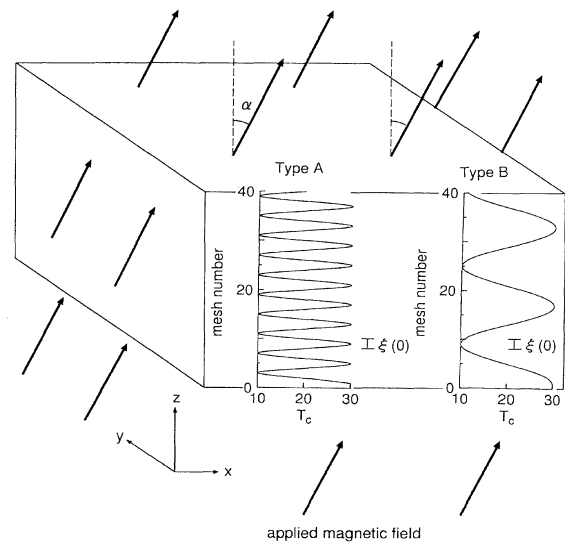


FIG. 1. The computational region of a rectangular parallelepiped superconductor. The variations of T_c in the z direction for type-A and type-B models and the coherence length $\xi_c(0)$ at zero temperature are shown in the figure. The external magnetic field is applied at an angle α in reference to the z direction.

$$\mathbf{j} = \sigma \left(-\nabla\varphi - \frac{1}{c} \frac{\partial \mathbf{A}}{\partial t} \right) + \text{Re} \left[\Delta^* \left(\frac{\nabla}{i} - \frac{2e}{\hbar c} \mathbf{A} \right) \Delta \right] \frac{\hbar c^2}{8\pi e \lambda^2}$$

$$= \mathbf{j}_n + \mathbf{j}_s = \frac{c}{4\pi} \text{rot rot} \mathbf{A},$$

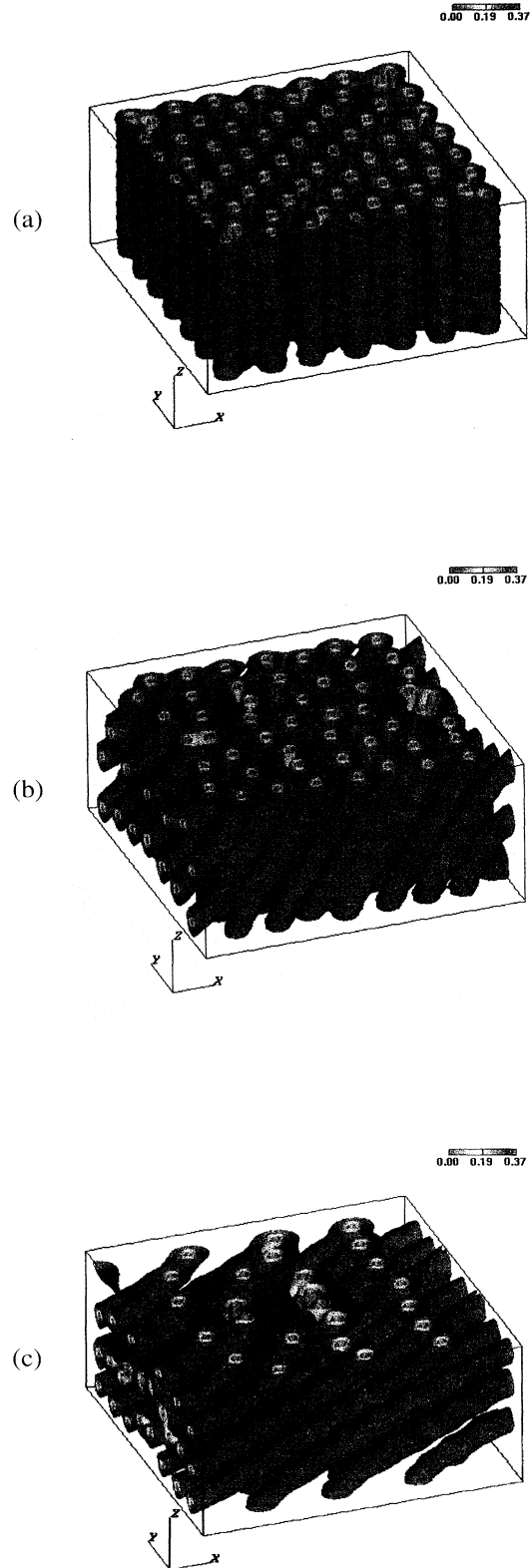
where Δ , \mathbf{A} , and φ are order parameter, vector, and scalar potential, and parameters D , ξ , and λ are diffusion constant, coherence, and penetration length, respectively. The \mathbf{j}_n and \mathbf{j}_s correspond to normal and superconducting current. The scaling method of these equations is found in Ref. [6], and the discretization using the link variable in Ref. [5].

The validity of these time-dependent equations is limited to dirty superconductors [9]. However, we employ the time development of these equations to achieve an equilibrium vortex state under the applied field. The obtained steady state is considered to realize the solution of the equilibrium GL equation coupled with the Maxwell equation. Therefore, the steady state results of the present numerical simulation can be applied to clean superconductors as well as dirty ones.

The computational region is a three-dimensional rectangular parallelepiped, and an external magnetic field is applied obliquely in reference to the c axis with an angle α as shown in Fig. 1. At the boundary, the gauge covariant first differential of the order parameter in the TDGL equation and the local magnetic field in the Maxwell equation are defined as $[(\nabla/i - 2e/\hbar c) \mathbf{A}]^2 \psi|_n = 0$ and $\mathbf{B} = \mathbf{H}_a$, where $|_n$ denotes the perpendicular direction at the boundary and \mathbf{H}_a is the external applied magnetic field. These boundary conditions are not realistic in the sense that an external magnetic field is uniformly applied at the surface without any diamagnetic effects. However, these conditions are sufficient for a small system or a system with many penetrating magnetic flux lines.

In the type- A and the type- B model, the critical temperature T_c is varied in the z direction (c axis) as $T_c = T_m + T_v \cos[(2\pi/d)z]$, where the mean critical temperatures T_m and T_v are assumed to be 20 and 10 K, respectively. The constant d denotes a unit length in the c axis of the lattice. Here, $d = 2.0\xi(0)$ is assumed for the type- A model and $d = 8.0\xi(0)$ for the type- B model as shown in Fig. 1. The mesh size of the three-dimensional region is $80 \times 80 \times 40$ and the smallest mesh is taken as $0.5\xi(0) \times 0.5\xi(0) \times 0.5\xi(0)$. The GL parameter κ and the time step Δt are taken as 2 and 0.01, respectively. In the present numerical simulation, thermal fluctuations are neglected. The external magnetic field is gradually applied

FIG. 2. (a) The snapshot of the spatial distribution of $|\psi|$ for $T = 10$ K, $H_a = 0.6H_{c2}$ (10 K), and 600 000 steps in the type- A model. In the figure, the value of $|\psi|$ changes from 0.00 (red) to 0.37 (green) and four isosurfaces are displayed. The colorless region near the boundary surface has a higher absolute value larger than 0.37 due to the strong superconducting surface state. (b) The snapshot of the spatial distribution of $|\psi|$ for $\alpha = 30^\circ$ in the type- A model. (c) The snapshot of the spatial distribution of $|\psi|$ for $\alpha = 60^\circ$ in the type- A model.



to the determined value during the first 100 000 steps to achieve the steady state, and the simulation is performed under the applied magnetic field. The magnetization is used to check whether the system reaches a steady state or not.

Figures 2(a), 2(b), and 2(c) show the numerical results of the steady vortex states for the type-A model with an external magnetic field of $0.6H_{c2}$ ($T = 10$ K) and the measured temperature of 10 K. The applied field is inclined in reference to the c axis (z direction) with an angle α of 0° , 30° , and 60° . Figure 2(a) shows the ordered vortex lattice state where the order parameter distribution along the vortex is modulated by the layered structure. However, as the external magnetic field inclines, it is observed that the ordered distribution of vortex at the surface becomes blurred. From Figs. 2(b) and 2(c), the flux lines are found to terminate perpendicularly at the surface due to the boundary conditions of the current at the surface. In the results of Fig. 2(c), for the external field applied nearly parallel to the layer, vortices have a tendency to align themselves because they are more stable in the weak superconducting layers [10].

Figures 3(a) and 3(b) show the internal structure of the vortex states with the inclined external magnetic field of $\alpha = 30^\circ$. Figure 3(a) shows the view from the y direction, and the disorder of vortex array is observed as marked in the figure. The enlarged view of this region is shown in Fig. 3(b) where the entangling of vortices occurs [11]. Figure 3(c) also shows the enlarged view of the region where the disorder of aligned vortices occurs in the case of $\alpha = 45^\circ$. These entangled vortex structures are found to be stable without thermal fluctuations, because they persist from the state which shows a constant magnetization. These entangled states are observed near the boundary wall of the computational region, and the merged segments of vortex lines exist in the weak superconducting region. Moreover, these phenomena are not found in the case of $\alpha = 0^\circ$. We found that the entanglement states appear due to the modification of inclined vortices near the sample edge.

It is predicted that these entangled states emerge as a result of the effect that the vortex bending, due to the presence of the sample edge and the layered structure, outdoes the intrinsic repulsive forces between vortices. In extensive type-II superconductors, it is considered that the vortex entangled state may also be observed near the irregular boundaries such as sample edge, rough surface, and grain boundary.

Figures 4(a) and 4(b) show the temperature dependence of the steady vortex states using the type-B model. Figures 4(a) and 4(b) are the simulation results at the temperature of 12 and 16 K, respectively. Here, the temperature is above T_c in the weak superconducting region. The external magnetic field and the angle α are taken as $0.6H_{c2}$ ($T = 12, 16$ K) and 45° , respectively. The bends in vortices due to the layered structure are clearly observed in Fig. 4(a), and the bending of these

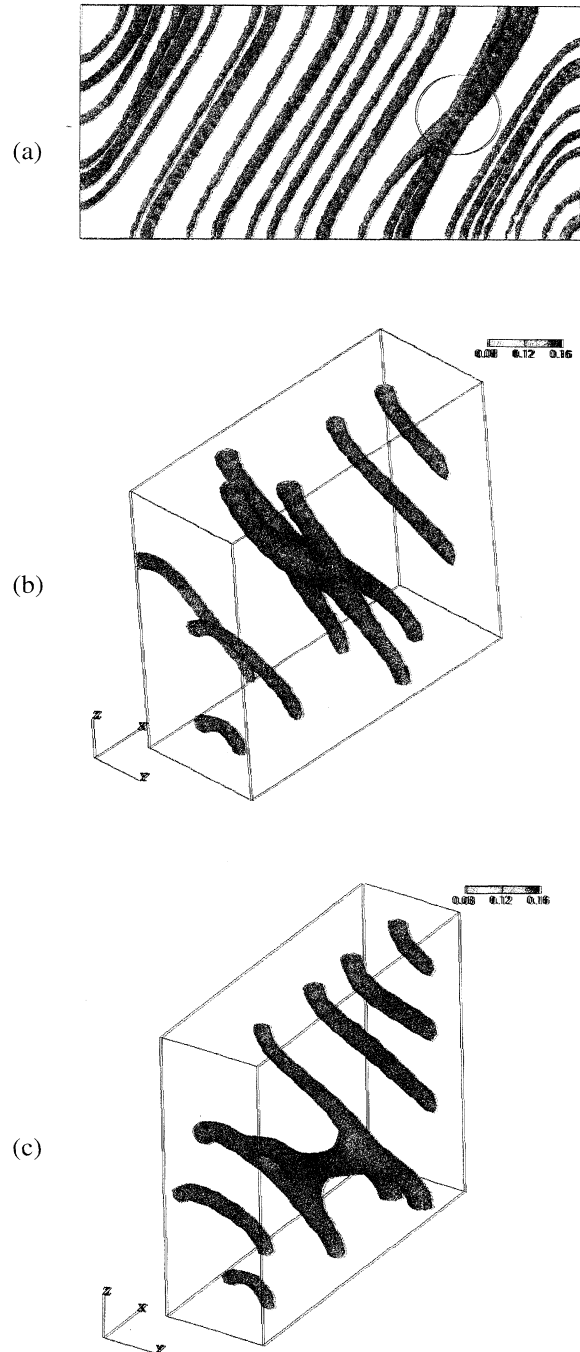


FIG. 3. (a) The snapshot of an isosurface of $|\psi| = 0.10$ for $T = 10$ K, $H_a = 0.6H_{c2}$ (10 K), $\alpha = 30^\circ$, and 1 000 000 steps in the type-A model. The view is from the y direction and the marked area shows a disorder of the vortex array. (b) The enlarged snapshot of the marked area in (a). (c) The enlarged snapshot of the vortex entangled state for $\alpha = 45^\circ$.

vortices becomes sharp as the temperature increases [12]. This result indicates a change from a straight vortex to a

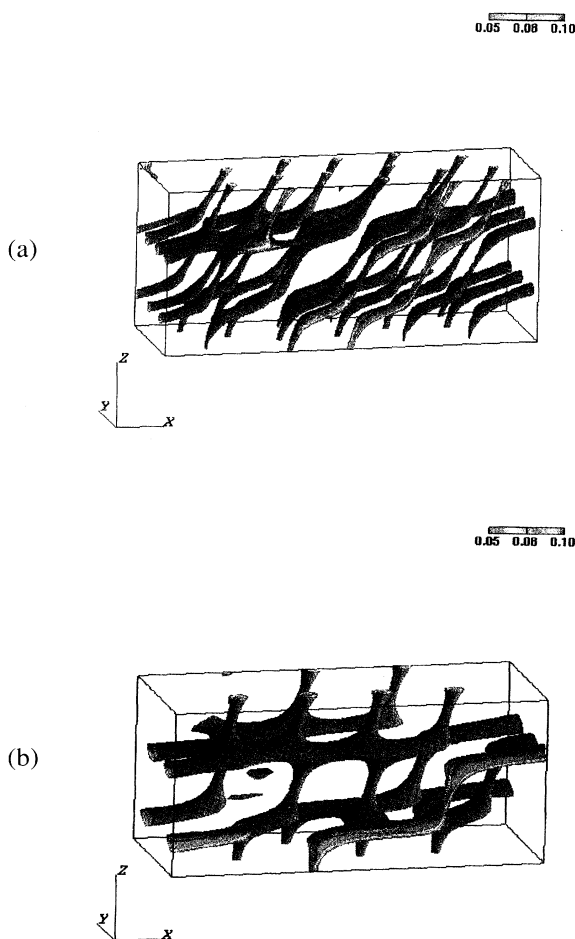


FIG. 4. (a) The cutaway view of the snapshot of the spatial distribution of $|\psi|$ for $T = 12$ K, $\alpha = 45^\circ$, and $H_a = 0.6H_{c2}$ ($T = 12$ K) in the type-*B* model. The value of $|\psi|$ changes from 0.05 (red) to 0.10 (green), and four color isosurfaces are displayed. (b) The snapshot of the spatial distribution of $|\psi|$ at 16 K in the type-*B* model, and other conditions are the same as in (a).

staircase vortex with segments parallel and perpendicular to the layer because the condensation energy loss, which arises from the existing vortices in each layer, changes as the temperature increases. In the type-*B* model, it is considered that the difference of the condensation energy loss between layers increases as the temperature increases, and the increasing difference gives rise to the change from bending vortex states to staircase vortex states. In Fig. 4(b), it is also seen that vortices in the weak superconducting layers exist parallel to the layers, while those in the strong superconducting region exist almost perpendicular to the layers. Moreover, the cross section of the vortices in the weak superconducting region becomes large due to the long coherence length, while tight and thin vortices are generated in the strong superconducting region. For the type-*A* model in the same conditions as

in Fig. 4(b), the absolute value of the superconducting order parameter falls to zero, except the surface and the bulk superconducting state is destroyed. The critical temperature in the presence of the applied field in the type-*B* model is found to be higher than that in the type-*A* model. The present numerical results in the type-*B* model strongly support the ideas of the staircase vortex [1] and the two-dimensional pancake vortex structures [2] predicted experimentally in high- T_c superconductors [3]. But, in the low temperature, it is also shown that there exists a range in which the sharpness of the vortex bending increases as the temperature increases.

In summary, a direct numerical simulation of the TDGL equation coupled with the Maxwell equation has been made to study steady flux line states for the layered superconductors. Using the modeled layered systems, a stable solution of entangled vortices for the coupled system of equations is shown to exist near the wall boundary. In particular, a crossover from the straight or the weakly bending vortex to the staircase vortex with segments parallel and perpendicular to the layers is found in the type-*B* model as the temperature increases. With these facts, we believe that the staircase and the pancake vortex structures exist in layered superconductors such as high- T_c materials and the other layered superconductors.

All these simulations have been carried out on the MONTE-4, a special purpose supercomputer for a particle system developed by the Japan Atomic Energy Research Institute (JAERI), and FUJITSU's VP2600 supercomputers. We would like to thank M. Akimoto, M. Tomiyama, and staff members for their support on massive calculations. We also thank K. Kato for computer graphics.

*On leave from FUJITSU Ltd., Izumi-Cho 1-2-4, Mito-Shi, Ibaraki-Ken, 310, Japan.

- [1] M. Tachiki and S. Takahashi, *Solid State Commun.* **72**, 1083 (1989).
- [2] P. H. Kes, J. Aarts, V. M. Vinokur, and C. J. van der Beek, *Phys. Rev. Lett.* **64**, 1063 (1990).
- [3] Z. X. Gao, E. Osquiguil, M. Maenhoudt, B. Wuyts, S. Libbrecht, and Y. Bruynseraede, *Phys. Rev. Lett.* **71**, 3210 (1993).
- [4] N. Nakamura, G. D. Gu, and N. Koshizuka, *Phys. Rev. Lett.* **71**, 915 (1993).
- [5] R. Kato, Y. Enomoto, and S. Maekawa, *Phys. Rev. B* **47**, 8016 (1993).
- [6] M. Machida and H. Kaburaki, *Phys. Rev. Lett.* **71**, 3206 (1993).
- [7] C. R. Hu and R. S. Thompson, *Phys. Rev. B* **6**, 110 (1972).
- [8] P. A. Mansky, P. M. Chaikin, and R. C. Haddon, *Phys. Rev. Lett.* **70**, 1323 (1993).
- [9] L. P. Gor'kov and G. M. Eliashberg, *Zh. Eksp. Teor. Fiz.* **54**, 612 (1968) [*Sov. Phys. JETP* **27**, 328 (1968)].
- [10] I. V. Grigorieva, J. W. Steeds, and K. Sasaki, *Phys. Rev. B* **48**, 16 865 (1993).
- [11] D. R. Nelson, *Phys. Rev. Lett.* **60**, 1973 (1988).
- [12] B. I. Ivlev, Yu. N. Ovchinnikov, and Yu. E. Pokrovsky, *Mod. Phys. Lett. B* **5**, 73 (1991).

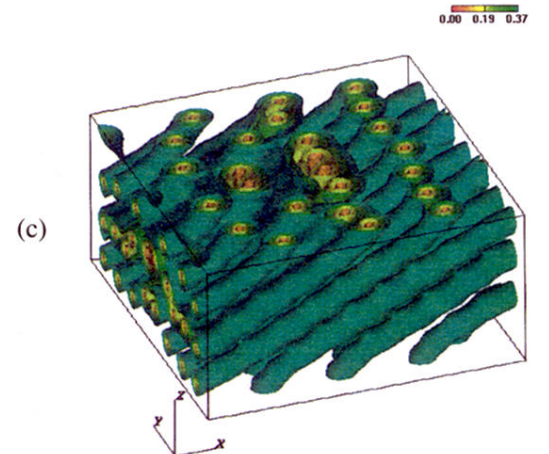
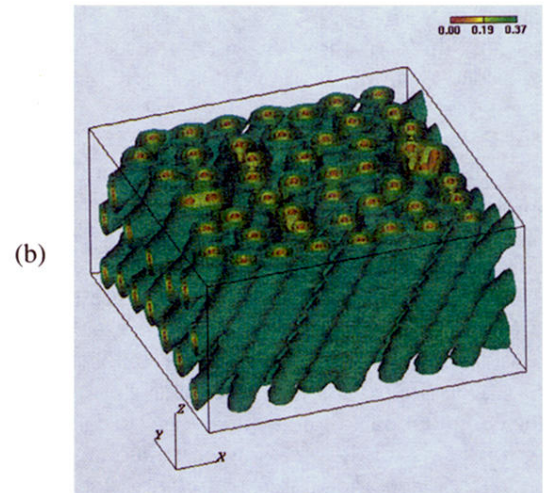
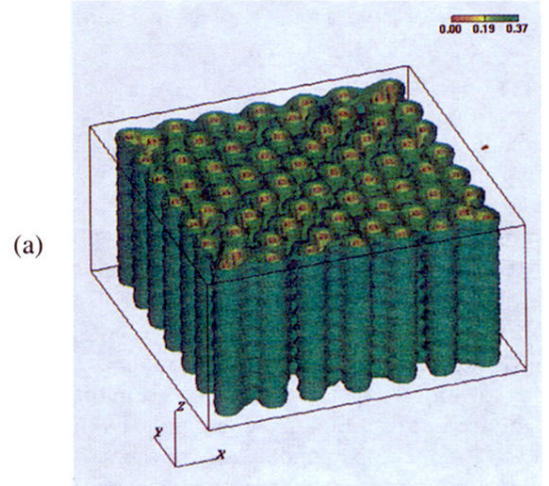


FIG. 2. (a) The snapshot of the spatial distribution of $|\psi|$ for $T = 10$ K, $H_a = 0.6H_{c2}$ (10 K), and 600 000 steps in the type-A model. In the figure, the value of $|\psi|$ changes from 0.00 (red) to 0.37 (green) and four isosurfaces are displayed. The colorless region near the boundary surface has a higher absolute value larger than 0.37 due to the strong superconducting surface state. (b) The snapshot of the spatial distribution of $|\psi|$ for $\alpha = 30^\circ$ in the type-A model. (c) The snapshot of the spatial distribution of $|\psi|$ for $\alpha = 60^\circ$ in the type-A model.

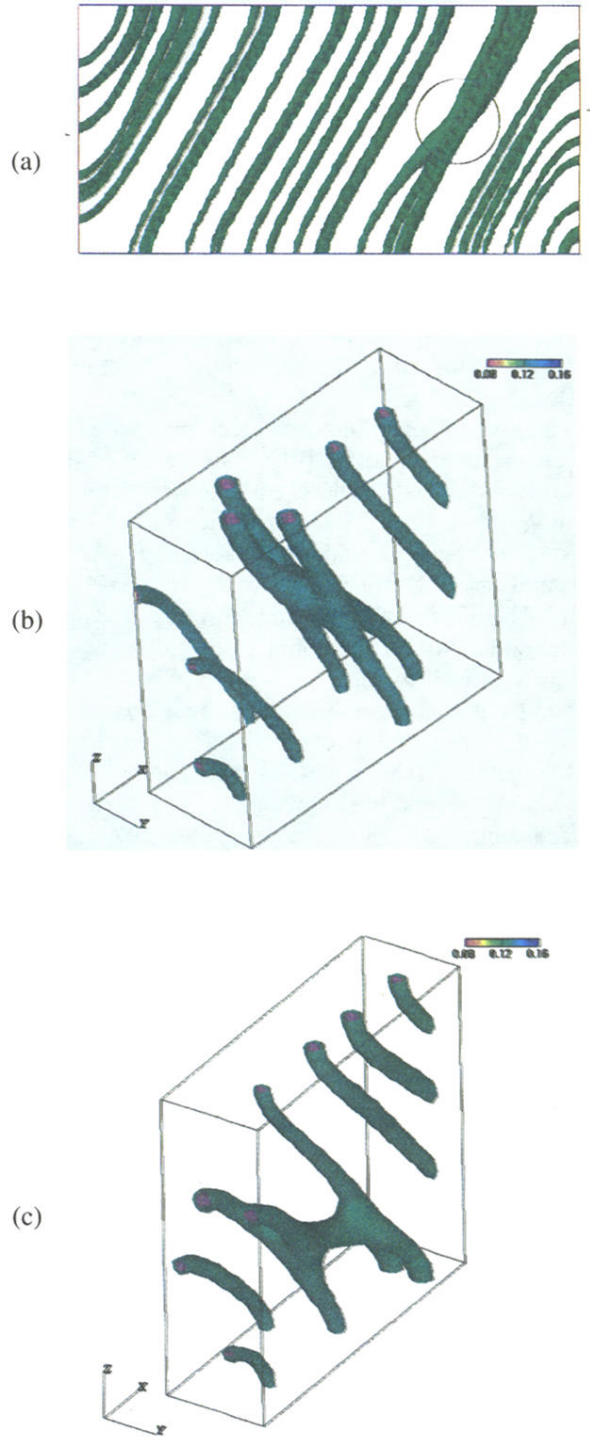


FIG. 3. (a) The snapshot of an isosurface of $|\psi| = 0.10$ for $T = 10$ K, $H_a = 0.6H_{c2}$ (10 K), $\alpha = 30^\circ$, and 1 000 000 steps in the type-A model. The view is from the y direction and the marked area shows a disorder of the vortex array. (b) The enlarged snapshot of the marked area in (a). (c) The enlarged snapshot of the vortex entangled state for $\alpha = 45^\circ$.

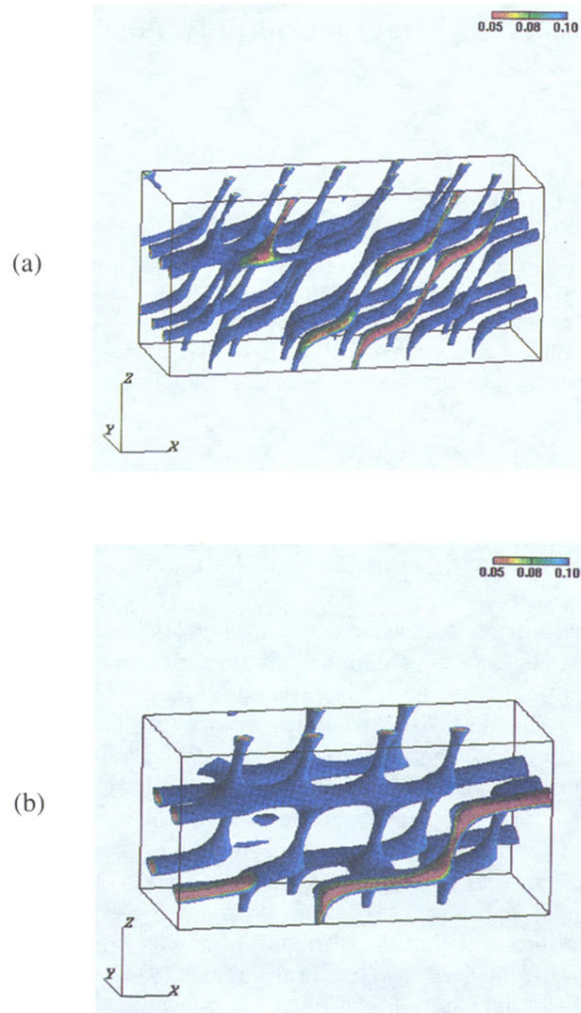


FIG. 4. (a) The cutaway view of the snapshot of the spatial distribution of $|\psi|$ for $T = 12$ K, $\alpha = 45^\circ$, and $H_a = 0.6H_{c2}$ ($T = 12$ K) in the type-*B* model. The value of $|\psi|$ changes from 0.05 (red) to 0.10 (green), and four color isosurfaces are displayed. (b) The snapshot of the spatial distribution of $|\psi|$ at 16 K in the type-*B* model, and other conditions are the same as in (a).